Enhanced MPC for Fast Frequency Control in Inverter-Dominated Power Systems

Ognjen Stanojev*, Uros Markovic*, Evangelos Vrettos‡, Petros Aristidou†, Duncan Callaway§, Gabriela Hug*
* EEH - Power Systems Laboratory, ETH Zurich, Physikstrasse 3, 8092 Zurich, Switzerland
† Department of Electrical Engineering, Computer Engineering and Informatics,
Cyprus University of Technology, Archiepiskopou Kyprianou 30, 3036 Limassol, Cyprus
‡ Swissgrid AG, Werkstrasse 10, 5080 Laufenburg, Switzerland
§ Energy & Resources Group, UC Berkeley, 310 Barrows Hall, Berkeley, CA 94720, US

***Abstract*—Due to the rising shares of renewable energy sources, future power systems are facing significant changes in control complexity and system inertia, thus making frequency regulation in power systems more challenging. This paper proposes a novel control scheme based on model predictive control for grid-forming Voltage Source Converters (VSCs), with the goal of exploiting their fast response capabilities and available DC-side energy storage to provide fast frequency control service to the system. An observer based on support vector machine regression detects and estimates system disturbances using only locally available measurements at each VSC. Frequency evolution is then anticipated through state-space predictions and the VSC power output is adjusted to compensate the disturbance and prevent frequency threshold violations. The proposed control scheme is evaluated and its effectiveness demonstrated through detailed time-domain simulations of the IEEE 39-bus test system.**

***Index Terms*—model predictive control, voltage source converter, frequency support, low-inertia systems, support vector regression**

I. Introduction

One of the key difficulties facing future power systems is the significant reduction in system inertia due to the rising shares of renewable energy sources and the concurrent decommissioning of conventional synchronous generators. As a result of this trend, system operation is challenged by faster frequency dynamics and higher Rate-of-Change-of-Frequency (RoCoF) following disturbances, which may lead to triggering of undesirable events such as load-shedding and blackouts [1]. Effective control of frequency in low-inertia systems can be achieved by complementing the conventional ancillary services with Fast Frequency Control (FFC) schemes [2], which can be provided by *grid-forming* Voltage Source Converters (VSCs) with controllable DC-side energy storage.

The existing literature on *grid-forming* converter control focuses mainly on a Virtual Synchronous Machine (VSM), i.e., an emulation technique based on the swing dynamics of a synchronous machine [3], and a droop-based control for regulating the converter's active and reactive power output [4]. However, while setting constant control parameters leads to satisfactory VSC performance under small frequency deviations, it prevents the converter from utilizing its maximum power capacity in emergency scenarios. Several studies have recently proposed improvements to the basic droop and VSM strategies through an adaptive adjustment of the controller gains according to the measured frequency imbalance. In particular, [5] proposes an online optimization algorithm, [6] uses an interval-based approach and [7] employs a linear quadratic regulator to adjust inertia and damping constants and keep the system frequency within limits after a disturbance. However, the proposed methods are not resilient to changes in system configuration and do not incorporate operational constraints in the control design. Furthermore, most of the previous work on VSM or droop-based VSC control focuses solely on the system's AC-side, considering the DC-link as an ideal storage element with an infinite amount of power and energy, thus neglecting potential storage limitations [8].

The behavior of these controllers can be optimized by means of Model Predictive Control (MPC), an optimization-based discrete time control scheme which has the possibility of incorporating operational constraints in the problem formulation while computing optimal control inputs based on state-space predictions [9]. Instead of adaptively adjusting the controller gains, the controller performance can be improved by altering the converter setpoints in response to a disturbance [10]–[12]. The work in [12] and [13] developed MPC-based controllers to improve the post-disturbance system behavior. Although the designed controllers have proven beneficial, the system representation was oversimplified by capturing only the swing equation dynamics and neglecting the specificity of converter-based generation. The aforementioned problems were partially addressed in [10] with an MPC-based frequency support through HVDC grids, where a *decentralized* MPC control scheme adapts the VSC output if constraint violations are detected or expected. This approach requires global information of grid topology and HVDC converter locations to calculate sensitivity factors corresponding to the DC-voltage droop and uses a simple frequency prediction model. Finally, the work in [11] addressed the aforementioned issues by developing *centralized* and *decentralized* MPC-based FFC strategies that can be incorporated as an additional layer to the primary frequency control (droop or VSM-based).

Inspired by *distributed* control, this paper improves upon the *decentralized* MPC from our previous work in [11] by developing an enhanced approach, where the controllers of individual VSCs exchange local measurements using communication links to cooperatively prevent any frequency threshold violations. A novel data-driven algorithm based on Support Vector Machine (SVM) regression is introduced for the disturbance estimation and frequency prediction. In comparison to *decentralized* FFC schemes currently available in the literature, a more accurate frequency prediction is achieved and hence a lower overall control effort is required for frequency containment. Nevertheless, this improvement comes at a cost of establishing communication links between the VSCs. Unlike traditional *centralized* approaches, which are prone to long computation times, reliability issues and commonly require wide-area measurements, the proposed approach uses only measurements locally available at each VSC and solves the MPC algorithm individually by each unit in parallel, thus attaining redundancy. However, more computational resources are required. Finally, in contrast to the studies in [10], [12], [13], where a simplified system model is used for dynamic simulations, the proposed control design is verified through time-domain simulations using a detailed dynamic model of a low-inertia system from [14].

978-1-7281-4701-7/20/$31.00

The remainder of the paper is structured as follows. Section II presents the proposed VSC control scheme with a supervisory layer that manages the FFC. Subsequently, Section III elaborates on the SVM regression model for disturbance estimation and the design of the enhanced controller. Simulation results and comparisons are illustrated in Section IV, whereas Section V draws the main conclusions of the study.

II. Fast Frequency Control Provision Using VSCs

Containment of substantial frequency excursions in events of large disturbances has conventionally been enabled by primary frequency control reserves together with sufficient rotational system inertia. However, with decreasing system inertia, traditional primary control reserves might not be fast enough to arrest the frequency excursions and hence, there is a need for new ancillary services operating at shorter timescales [2]. This paper focuses on fast frequency control which is characterized by a rapid power delivery of the providing units and whose aim is to improve the transient response by controlling RoCoF and nadir values of the system frequency response. Converter-interfaced generators with the associated energy buffers are the most suitable units for FFC provision due to their fast response times, high efficiency and reliability. Commonly, a two-level VSC control scheme comprising inner and outer control loops with employed VSM or droop-based active power control is used in the literature. The FFC functionality can be improved by extending it with a supervisory control layer which solely manipulates setpoints of the power controllers.

A. Voltage Source Converter Model

A three-phase two-level VSC model considered in this study is composed of a DC-side circuit, an AC subsystem and a lossless switching unit which transforms the DC-capacitor voltage $v_{\mathrm{dc}} \in \mathbb{R}_{>0}$ into an AC voltage $v_{\mathrm{sw}}^{abc} \in \mathbb{R}^3$ based on the modulation signal $m \in [-\mathbb{1}_3, \mathbb{1}_3]$, as depicted in Fig. 1, with the mathematical model defined in per unit.

The DC-side circuit is comprised of a DC-link capacitor $c_{\mathrm{dc}} \in \mathbb{R}_{>0}$, a constant current source $i_{\mathrm{dc}}^\star \in \mathbb{R}$ modeling the input of the renewable generation and a controllable DC current source $\bar{i}_{\mathrm{dc}} \in \mathbb{R}$ representing flexibility of the associated energy storage system

$$c_{\mathrm{dc}}\dot{v}_{\mathrm{dc}} = i_{\mathrm{dc}}^\star + \bar{i}_{\mathrm{dc}} - i_{\mathrm{in}}, \tag{1a}$$
$$\dot{\chi} = \bar{i}_{\mathrm{dc}}/e_b, \tag{1b}$$

with $e_b \in \mathbb{R}_{>0}$ denoting the total energy capacity of the battery, $\chi \in \mathbb{R}_{>0}$ designating the battery State-of-Charge (SoC) and $i_{\mathrm{in}} \in \mathbb{R}_{>0}$ representing the input current.

The AC-side model and the VSC control scheme are implemented in a Synchronously-rotating Reference Frame (SRF), with the dq-frame quantities described in vector[1] form $x := (x^d, x^q) = T(\theta_r)x^{abc}$, $T(\theta_r)$ representing the power-variant dq-transform and $\theta_r \in [-\pi, \pi)$ being a reference angle. The AC subsystem comprises an RLC filter $(r_f, \ell_f, c_f) \in \mathbb{R}^3_{>0}$ and a transformer equivalent $(r_t, \ell_t) \in \mathbb{R}^2_{>0}$ and can be described by

$$\dot{i}_f = \omega_b \ell_f^{-1}(v_{\mathrm{sw}} - v_f) - \big(\omega_b r_f \ell_f^{-1} + j\omega_b\omega_r\big) i_f, \tag{2a}$$
$$\dot{v}_f = \omega_b c_f^{-1}(i_f - i_g) - j\omega_b\omega_r v_f, \tag{2b}$$
$$\dot{i}_g = \omega_b \ell_t^{-1}(v_f - v_t) - \big(\omega_b r_t \ell_t^{-1} + j\omega_b\omega_r\big)\, i_g, \tag{2c}$$

[1]Note that for column vectors $x \in \mathbb{R}^n$ and $y \in \mathbb{R}^m$ we use $(x, y) = \big[x^\mathsf{T}, y^\mathsf{T}\big]^\mathsf{T} \in \mathbb{R}^{n+m}$ to denote a stacked vector.

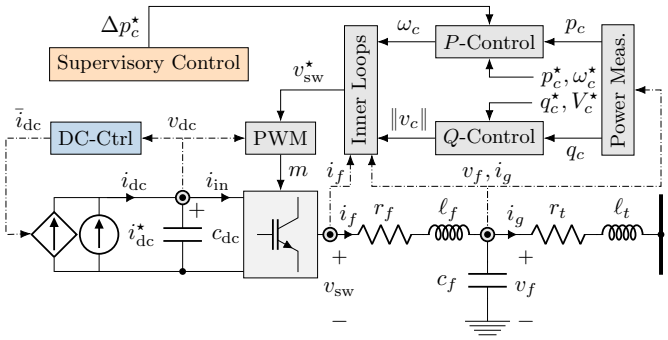

Fig. 1. Proposed control structure, with the added supervisory layer shown in orange.

where $i_f \in \mathbb{R}^2$ and $v_f \in \mathbb{R}^2$ are the filter current and voltage, $v_t \in \mathbb{R}^2$ is the voltage at the connection terminal, and $i_g \in \mathbb{R}^2$ denotes the transformer current; the system base frequency is represented by $\omega_b \in \mathbb{R}$ and $\omega_r \in \mathbb{R}_{>0}$ is the normalized reference for the angular velocity of the dq-frame.

B. Control Implementation

The outer control loop consists of active and reactive power controllers (denoted by P- and Q-Control in Fig. 1) providing the output voltage magnitude $\|v_c\| \in \mathbb{R}$ and frequency $\omega_c \in \mathbb{R}$ references by adjusting the predefined setpoints $(p_c^\star, \omega_c^\star, q_c^\star, V_c^\star) \in \mathbb{R}^4$ according to the droop control law and the power measurements $p_c := v_f^\mathsf{T} i_g$ and $q_c := v_f^\mathsf{T} J i_g$, as follows:

$$\omega_c := \omega_c^\star + R_c^p(p_c^\star + \Delta p_c^\star - \tilde{p}_c), \quad \dot{\tilde{p}}_c := \omega_f(p_c - \tilde{p}_c), \tag{3a}$$
$$\|v_c\| := V_c^\star + R_c^q(q_c^\star - \tilde{q}_c), \qquad \dot{\tilde{q}}_c := \omega_f(q_c - \tilde{q}_c), \tag{3b}$$

with $J \in \mathbb{R}^2$ indicating the 90° rotation matrix, $R_c^p \in \mathbb{R}_{>0}$ and $R_c^q \in \mathbb{R}_{>0}$ denoting the active and reactive power droop gains, $\tilde{p}_c \in \mathbb{R}$ and $\tilde{q}_c \in \mathbb{R}$ representing the low-pass filtered active and reactive power measurements, $\omega_f \in \mathbb{R}$ being the low-pass filter cut-off frequency and $\Delta p_c^\star \in \mathbb{R}$ indicates the setpoint change generated by the supervisory layer. Moreover, the internal RoCoF state can be obtained by taking the derivative of (3a), which yields

$$\dot{\omega}_c = R_c^p \omega_f(\tilde{p}_c - p_c). \tag{4}$$

The outputs of the active and reactive power controllers are then passed to the inner control loops comprising a cascade of voltage and current controllers, which compute the switching voltage reference $v_{\mathrm{sw}}^\star \in \mathbb{R}^2$. More precisely, the inner loops consist of a PI voltage controller

$$\dot{\xi} = v_f^\star - v_f, \tag{5a}$$
$$i_f^\star = K_P^v(v_f^\star - v_f) + K_I^v \xi + K_F^v i_g + j\omega_c c_f v_f, \tag{5b}$$

that provides a reference $i_f^\star \in \mathbb{R}$ for the current PI controller

$$\dot{\gamma} = i_f^\star - i_f, \tag{6a}$$
$$v_{\mathrm{sw}}^\star = K_P^i(i_f^\star - i_f) + K_I^i \gamma + K_F^i v_f + j\omega_c \ell_f i_f, \tag{6b}$$

where $(K_P^v, K_P^i) \in \mathbb{R}^2_{>0}$, $(K_I^v, K_I^i) \in \mathbb{R}^2_{\geqslant 0}$ and $(K_F^v, K_F^i) \in \mathbb{Z}^2_{\{0,1\}}$ are the respective proportional, integral, and feed-forward gains, $\xi \in \mathbb{R}^2$ and $\gamma \in \mathbb{R}^2$ represent the integrator states, and superscripts v and i denote the voltage and current controllers. Finally, we assume that the modulation voltage reference signal $v_{\mathrm{sw}}^\star$ is perfectly transformed to the AC side, i.e. $v_{\mathrm{sw}} := v_{\mathrm{sw}}^\star$.

In terms of the DC-side regulation, a PI controller is employed to keep the capacitor voltage at a predefined reference value $v_{\mathrm{dc}}^{\star} \in \mathbb{R}_{>0}$ using the flexibility of the DC-side storage:

$$\dot{\nu} = v_{\mathrm{dc}}^{\star} - v_{\mathrm{dc}}, \tag{7a}$$

$$\bar{i}_{\mathrm{dc}} = K_P^{\mathrm{dc}}(v_{\mathrm{dc}}^{\star} - v_{\mathrm{dc}}) + K_I^{\mathrm{dc}}\nu + K_F^{\mathrm{dc}} i_{\mathrm{dc}}^{\star}, \tag{7b}$$

where $\nu \in \mathbb{R}$ represents the integrator state and $K_P^{\mathrm{dc}} \in \mathbb{R}$, $K_I^{\mathrm{dc}} \in \mathbb{R}$ and $K_f^{\mathrm{dc}} \in \mathbb{R}$ are the proportional, integral and feed-forward gains, respectively.

Finally, based on the optimal control algorithm discussed in more detail in Section III, the supervisory control layer generates a signal $\Delta p_c^{\star} \in \mathbb{R}$ in order to adjust the active power setpoint in (3a) in response to a detected disturbance.

III. Optimal Control Design

The proposed supervisory control layer is based on an optimal control strategy and consists of a trigger circuit, a disturbance estimation algorithm and a model predictive controller, as shown in Fig. 2. The converters $i \in \mathcal{I}$ participating in FFC are linked with communication lines used for the exchange of local measurements pertaining to active power, SoC and frequency, described by the vector $\tilde{x} = (p_{c_i}, \chi_i, \omega_{c_i}) \in \mathbb{R}^3$, as well as the estimated maximum instantaneous RoCoF values $\dot{\omega}_m \in \mathbb{R}$ among the participating inverter units. As the focus of this work is on control design, the communication network is assumed to have fully connected topology and operate via optical-fibre cables with signal delays below $100\,\mathrm{ms}$ [15].

The trigger circuit ensures that the proposed FFC scheme remains inactive during normal operation and activates only in emergency situations. Since large disturbances are accompanied by large RoCoF values, internally obtainable RoCoF estimates given by (4) are used as indicators. As long as the RoCoF stays below a predefined threshold $\bar{\varepsilon}_{\omega} \in \mathbb{R}_{>0}$ the controller remains idle. Once the threshold is violated, the trigger circuit generates an "on" signal and keeps the MPC algorithm running until the average RoCoF value $\langle \dot{\omega}_c \rangle$ falls below a prescribed margin $\underline{\varepsilon}_{\omega} \in \mathbb{R}_{>0}$ when an "off" signal deactivates the algorithm. Since RoCoF variations have a fast system-wide propagation, FFC schemes of all VSCs are triggered simultaneously and hence, operate synchronously. The trigger circuit also activates the disturbance estimation algorithm which identifies the maximum instantaneous local RoCoF and uses SVM regression to estimate the disturbance magnitude required for the frequency prediction model.

A. Frequency Prediction Model

The work in [7] derived a Center-of-Inertia (CoI) frequency model of a generic low-inertia system comprised of both synchronous and converter-based generators. In Laplace domain it can be represented by a simplified transfer function $G(s)$ relating the system frequency deviation $\Delta f(s) \in \mathbb{C}$ to a change in power $\Delta p(s) \in \mathbb{C}$, with the inclusion of inertial response and primary frequency control. This resulting function is

$$G(s) = \frac{\Delta f(s)}{\Delta p(s)} = \frac{1}{MT}\frac{1 + sT}{s^2 + 2\zeta\omega_n s + \omega_n^2}. \tag{8}$$

The natural frequency $\omega_n \in \mathbb{R}_{>0}$ and damping ratio $\zeta \in \mathbb{R}_{>0}$ are computed as follows

$$\omega_n = \sqrt{\frac{D + R_g}{MT}}, \quad \zeta = \frac{M + T(D + F_g)}{2\sqrt{MT(D + R_g)}}, \tag{9}$$

with parameters $R_g \in \mathbb{R}_{>0}$ and $F_g \in \mathbb{R}_{>0}$ denoting the average inverse droop control gain and fraction of total power generated by the high-pressure turbines of Synchronous Generators (SGs), $T \in \mathbb{R}_{>0}$ representing the generator time constant and $M \in \mathbb{R}_{>0}$ and $D \in \mathbb{R}_{>0}$ designating the weighted system averages of inertia and damping constants, respectively. For more details and verification of the proposed frequency model, the reader is referred to [7].

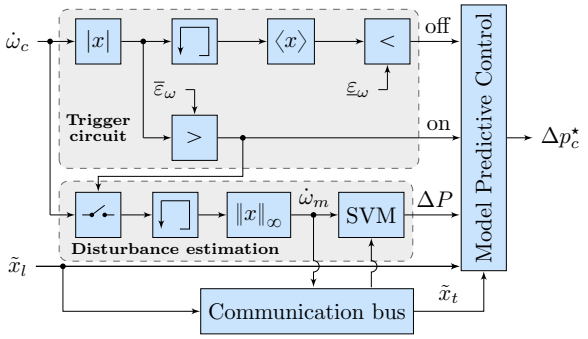

Fig. 2. Structure and composing elements of the proposed supervisory control layer.

Transfer function (8) can now be transformed into a controllable canonical state-space model of the form:

$$\underbrace{\begin{bmatrix}\dot{q}_1(t)\\ \dot{q}_2(t)\end{bmatrix}}_{\dot{x}} = \underbrace{\begin{bmatrix}0 & 1\\ -\omega_n^2 & -2\zeta\omega_n\end{bmatrix}}_{A}\begin{bmatrix}q_1(t)\\ q_2(t)\end{bmatrix} + \underbrace{\begin{bmatrix}0\\ 1\end{bmatrix}}_{B}\Delta p(t), \tag{10a}$$

$$\Delta f(t) = \underbrace{\begin{bmatrix}\frac{1}{MT} & \frac{1}{M}\end{bmatrix}}_{C}\begin{bmatrix}q_1(t)\\ q_2(t)\end{bmatrix}, \tag{10b}$$

where $A \in \mathbb{R}^{2\times 2}$, $B \in \mathbb{Z}_{\geqslant 0}^2$ and $C^{\mathsf{T}} \in \mathbb{R}_{\geqslant 0}^2$ are the state-space matrices, and $x := (q_1, q_2) \in \mathbb{R}^2$ denotes the state vector, where elements q_1 and q_2 have no physical interpretation. The model is time-invariant and can be parametrized using the system identification procedure presented in [11].

B. Disturbance estimation

The model in (10) requires the disturbance signal $\Delta p(t) \in \mathbb{R}$ to be known in order to predict the frequency evolution. This work focuses solely on generator and load loss disturbances which can be modeled by the step function of magnitude $\Delta P \in \mathbb{R}$. In [11], we presented a decentralized MPC based on the model in (10) and used a well-known relationship between the maximum instantaneous RoCoF $\dot{\omega}_{\max}$ and the disturbance magnitude ΔP for local disturbance estimation of the form $\Delta P = -M\dot{\omega}_{\max}$. However, considering that different disturbances across the system can result in the same RoCoF values measured at a single node in the system, this technique often leads to incorrect disturbance estimates.

The disturbance estimation quality can be improved by means of an observer of the following form

$$\Delta P = f(\dot{\omega}_{\max_1}, \dot{\omega}_{\max_2}, \ldots, \dot{\omega}_{\max_n}), \tag{11}$$

where $n := \|\mathcal{I}\| \in \mathbb{Z}_{>0}$ is the number of inverters participating in FFC and $f : \mathbb{R}^n \mapsto \mathbb{R}$ represents a nonlinear map determined by SVM regression [16]. Training data $\{(\Phi_1, \Delta P_1), (\Phi_2, \Delta P_2), \ldots, (\Phi_d, \Delta P_d)\} \subset \mathbb{R}^{(n+1)}$ for SVM regression is obtained by performing *offline* simulations for $d \in \mathbb{Z}_{>0}$ disturbances at different nodes in the system and storing the instantaneous RoCoF measurements for all n inverters $\Phi = (\dot{\omega}_{\max_1}, \dot{\omega}_{\max_2}, \ldots, \dot{\omega}_{\max_n}) \in \mathbb{R}^n$. The goal of support vector regression is to find a function that has at most $\varepsilon \in \mathbb{R}_{>0}$

deviation from the obtained targets for all training data, which is at the same time as flat as possible. Basis functions (kernels) are used to map the training set from the input space into higher dimensional spaces, called feature spaces, where linear relationships between input and output data can be achieved. In this work, we use the Radial-Basis-Function (RBF) kernel of the form $k(\Phi, \Phi') = e^{-(\gamma\|\Phi-\Phi'\|_2)^2}$, where $\gamma \in \mathbb{R}$ is a free parameter. A linear model can subsequently be solved in the feature space to obtain parameters $w \in \mathbb{R}^n$ and $b \in \mathbb{R}$ of the function $f(\Phi) = \langle w, \Phi \rangle + b$, with $\langle \cdot \rangle$ denoting the inner product. Although the optimization problem at hand is computationally simpler to solve in its Lagrange dual form, for brevity and compactness of presentation we present here the primal problem

$$\min_{w,b,\xi,\nu} \quad \|w\|^2 + C \sum_{j=1}^{d} (\xi_j + \nu_j) \tag{12a}$$

$$\text{s.t} \quad \Delta P_j - \langle w, \Phi_j \rangle - b \leqslant \varepsilon + \xi_j, \quad j = 1, 2, \ldots, d, \tag{12b}$$

$$\langle w, \Phi_j \rangle + b - \Delta P_j \leqslant \varepsilon + \nu_i, \quad j = 1, 2, \ldots, d, \tag{12c}$$

$$\xi_j \geqslant 0, \nu_j \geqslant 0, \quad j = 1, 2, \ldots, d, \tag{12d}$$

with $\xi_j \in \mathbb{R}$ and $\nu_j \in \mathbb{R}$ representing slack variables and $C \in \mathbb{R}$ denoting the error penalty. Finally, a mapping $\Delta P = f(\Phi)$ is obtained and represented by the SVM block in Fig. 2.

C. MPC Problem Formulation

The proposed MPC formulation aims to minimize the total control effort over all time steps $\mathcal{H} = \{\hat{k}, \hat{k}+1, \ldots, \hat{k}+N\}$ within the MPC prediction horizon N, with $\hat{k}$ being the current time step. It is solved individually for each unit $i \in \mathcal{I}$ in order to obtain the optimal setpoint change $\Delta p^{\star}_{c_i}(\hat{k}+1)$ for the next time step, and is formulated as follows:

$$\min_{\Delta p^{\star}, \eta_f, \eta_r} \quad \left\| C_P^{\mathsf{T}} \Delta p^{\star} \right\| + C_H \left(\|\eta_f\|_{\infty} + \|\eta_r\|_{\infty} \right) \tag{13a}$$

$$\text{s.t.} \quad \forall k \in \mathcal{H}, \forall i \in \mathcal{I},$$

$$x(k+1) = A_d x(k) + B_d(\Delta p^{\star}(k) + \Delta P), \tag{13b}$$

$$f(k) = C_d x(k) + f_0, \tag{13c}$$

$$\dot{f}(k) = (f(k) - f(k-1))/T_s, \tag{13d}$$

$$\Delta p^{\star}_{c_i}(k) = (P_{n_i}/P_t)\Delta p^{\star}(k), \tag{13e}$$

$$p_{c_i}(k) = p^{\star}_{c_i} + \sum_{r=1}^{k} \Delta p^{\star}_{c_i}(r) + R^p_{c_i}(\omega^{\star}_{c_i} - \omega(k)), \tag{13f}$$

$$\chi_i(k+1) = \chi_i(k) + T_s(p^{\star}_{c_i} - p_{c_i}(k))/e_{b_i}, \tag{13g}$$

$$\underline{p}_{c_i,\text{lim}} \leqslant p_{c_i}(k) \leqslant \bar{p}_{c_i,\text{lim}}, \tag{13h}$$

$$\underline{\chi}_{i,\text{lim}} \leqslant \chi_i(k) \leqslant \bar{\chi}_{i,\text{lim}}, \tag{13i}$$

$$\underline{f}_{\text{lim}} \leqslant f(k) + R^p_{c_i}\Delta p^{\star}_{c_i}(k) \leqslant \bar{f}_{\text{lim}}, \tag{13j}$$

$$\underline{f}_{\text{lim}} - \eta_f(k) \leqslant f(k) \leqslant \bar{f}_{\text{lim}} + \eta_f(k), \tag{13k}$$

$$\underline{\dot{f}}_{\text{lim}} - \eta_r(k) \leqslant \dot{f}(k) \leqslant \bar{\dot{f}}_{\text{lim}} + \eta_r(k), \tag{13l}$$

$$\eta_f(k) \geqslant 0, \eta_r(k) \geqslant 0, \tag{13m}$$

with $\Delta p^{\star} \in \mathbb{R}^N$ denoting the vector of total setpoint change required for disturbance compensation, $\eta_f \in \mathbb{R}^N_{\geqslant 0}$ and $\eta_r \in \mathbb{R}^N_{\geqslant 0}$ being vectors of slack variables for each time step. The cost of the converter action $C_P \in \mathbb{R}^N_{>0}$ coefficients at each time step k are chosen such that $C_P(k) \leqslant C_P(k+1)$ holds which incentivizes the use of control resources at earlier time steps in order to prevent late reactions and frequency oscillations near the frequency limit. Large penalty factor $C_H \in \mathbb{R}_{>0}$ on the norm of slack variables is introduced to relax the respective frequency and RoCoF constraints and avoid infeasibility.

The prediction model described in (13b)-(13d) is the zero-order hold equivalent of the frequency prediction model in (10), with $A_d \in \mathbb{R}^{2\times 2}$, $B_d \in \mathbb{Z}^2_{>0}$ and $C_d^{\mathsf{T}} \in \mathbb{R}^2_{>0}$ describing the respective state space, $T_s \in \mathbb{R}_{>0}$ designating the prediction time step length, and $f_0 \in \mathbb{R}_{>0}$ representing the frequency linearization point. Equality (13d) augments the system frequency model with the prediction of average RoCoF over a single time step.

The availability of local measurements of other VSCs, communicated between the inverters at every time step as depicted in Fig 2, can be exploited to predict their behavior. Each VSC participating in FFC is expected to compensate a portion of the total disturbance and hence, the computed total setpoint change $\Delta p^{\star}$ is weighted by P_{n_i}/P_t, with $P_{n_i} \in \mathbb{R}_{>0}$ being the rated power of the VSC i and $P_t \in \mathbb{R}_{>0}$ representing the net installed power of all VSCs.

Constraints (13f)-(13j) predict potential physical limitations of each VSC i such as the limits on power output $p_{c_i}(k)$. Note that VSC setpoints $(p^{\star}_{c_i}, \omega_{c_i})$ and droop gain parameters R_{c_i} might change during operation, thus need to be exchanged through communication network as well. Equation (13g) represents a simple prediction model of the battery SoC based on the difference between the output power and the initial power setpoint. Expression (13j) captures the impact of droop control on the system frequency, thus anticipating excessive frequency spikes coming from fast setpoint changes at the inverter nodes and preventing potential converter tripping. Finally, constraints (13k)-(13l) impose upper and lower bounds on system frequency and RoCoF, with superscripts "min" and "max" indicating the respective lower and upper thresholds; (13m) imposes non-negativity constraints on slack variables.

IV. Results

The proposed control scheme has been tested and evaluated on a modified version of the IEEE 39-bus New England test system [17] depicted in Fig. 3. For purposes of this

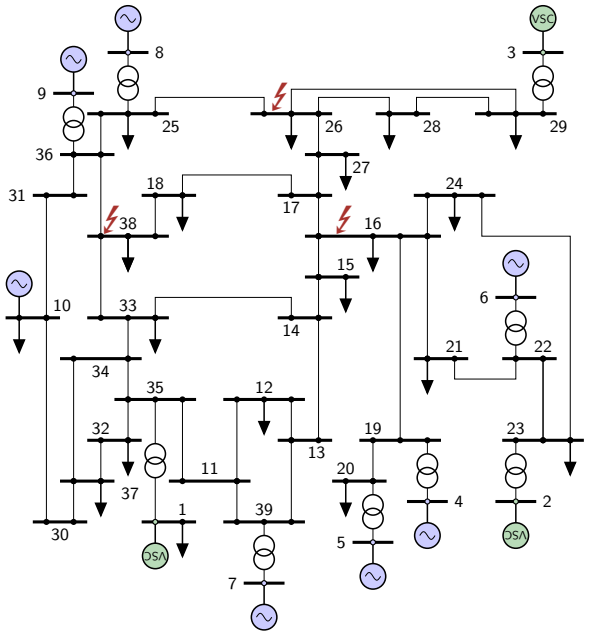

Fig. 3. IEEE 39-bus New England test system, with inverter-based generation placed at nodes 1, 2 and 3. Disturbance locations under consideration are indicated by red symbols.

study, the system has been modified by replacing SGs at nodes 1, 2 and 3 by converter-interfaced units with 1000 MW installed power and 10 MWh battery energy storage capacity. All VSCs are equipped with the control scheme presented in Section II. The system has been implemented in MATLAB using a differential-algebraic equation power system model previously introduced in [14], comprising detailed models of both synchronous and inverter-based generation as well as transmission network dynamics.

The disturbances considered in this work are loss of a generator and loss of a load, which can be simulated through step-changes in active power at network buses of interest. The first stage of automatic load-shedding is assumed to occur in case of frequency deviation beyond ± 0.5 Hz. The RoCoF protection is set to trigger at ± 1 Hz/s for RoCoF measurements averaged over a 250 ms cycle. Consequently, the limits f_{lim} and f_{lim} in (13) are set to ± 0.5 Hz and ± 1 Hz/s, respectively. Minimum and maximum power output and state of charge thresholds are set to 0 and 1 respectively, since the model is defined in per unit. The MPC-based controller operates at a constant time step of 250 ms to account for communication delays and MPC computation time. The prediction horizon of three time steps was chosen to reflect a trade-off between controller performance and computational effort. Since power ratings of all VSCs are the same, each unit is expected to participate with an equal share in disturbance mitigation.

A training data set was created by simulating 350 disturbances at different nodes in the system with various disturbance magnitudes for the purpose of SVM regression learning of the function in (11). The obtained prediction model shows an overall *RMSE* of 1.88 %, with the following parameters: $\epsilon = 0.0024$, $\gamma = 0.52$, $C = 9.54$ and $b = -1.81$.

A. Control Performance & Comparison

In this section, we analyze the performance of the proposed control and compare it to the decentralized approach from [11], where the disturbances are estimated locally as described in Section III-B. Locations of considered disturbances and their magnitudes are listed in Table I, along with the disturbance estimations using the SVM regression model and decentralized local estimates for each VSC.

Let us first consider a power disturbance of 1575 MW at node 16. Frequencies and power outputs of individual generators for both FFC approaches are showcased in Fig. 4, as well as the "worst-case" generator frequency when the FFC supervisory layer is inactive. The enhanced controller efficiently contains the frequency as a result of accurate disturbance estimation using resources of all 3 inverters equally. On the other hand, the decentralized VSC controller at node 3 remains inactive due to the large electrical distance to the fault and the consequent underestimation of the disturbance. However, the support from the other two converters is sufficient for successful frequency containment.

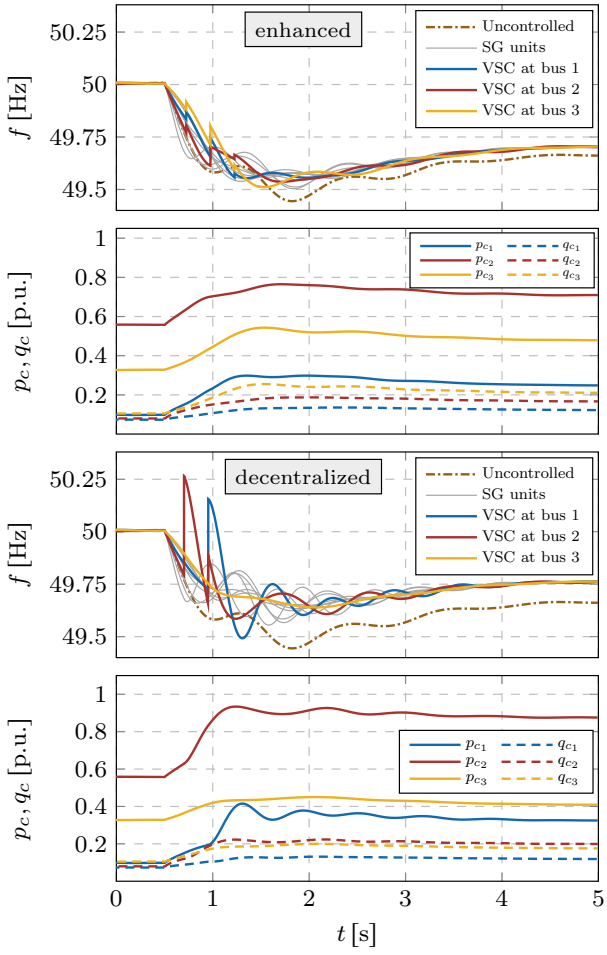

Fig. 4. Individual unit frequency response for the enhanced (top) and decentralized (bottom) FFC schemes following a disturbance at bus 16. Dashed line depicts the worst case generator frequency without the FFC.

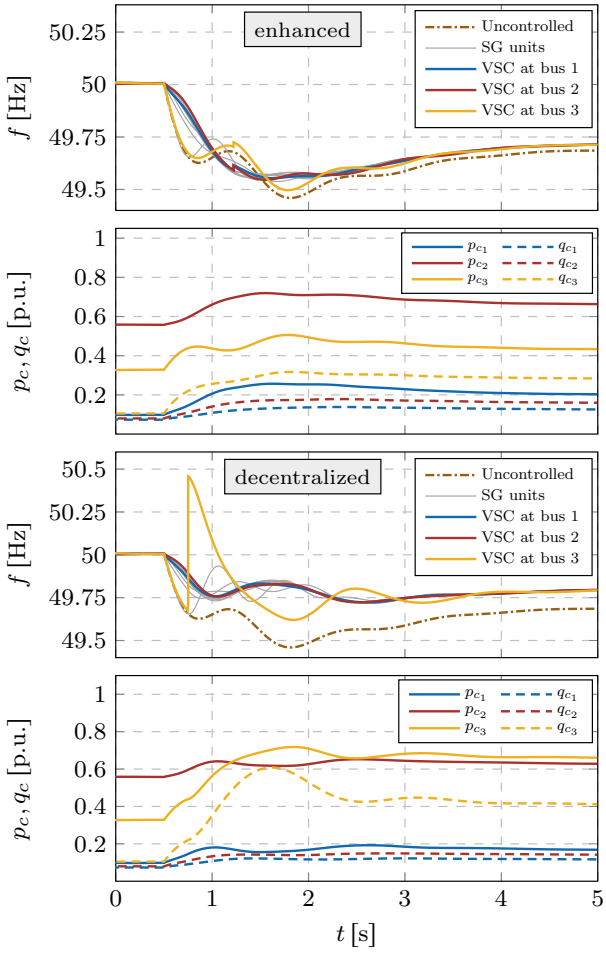

Fig. 5. Individual unit frequency responses for the enhanced (top) and decentralized (bottom) FFC schemes following a disturbance at bus 26. Dashed line denotes the worst case generator frequency without the FFC.

TABLE I
POWER DISTURBANCE SCENARIOS AT DIFFERENT BUSES WITH INDICATED APPLIED DISTURBANCE MAGNITUDES AND ESTIMATED DISTURBANCE VALUES THROUGH SVM AND DECENTRALIZED ESTIMATION TECHNIQUES.

Bus	$\Delta P^{\star}$ [**MW**]	ΔP_{SVM} [**MW**]	ΔP_{dec} [**MW**]		
			VSC 1	VSC 2	VSC 3
16	1575	1578.7	1550	1955	835
26	1430	1433.4	1100	790	3860
38	1850	1845.3	1390	520	650

Controller performance for a disturbance of 1430 MW at bus 26, which is located in the vicinity of several generators, is illustrated in Fig. 5. In this scenario, only a small contribution from the VSCs is needed for frequency containment, as shown by the enhanced control approach. The VSC at node 3 overestimates the disturbance and overreacts in the decentralized approach, whereas the other two VSCs remain idle.

Lastly, we consider a disturbance of 1850 MW at bus 38 which is located a large electrical distance away from all three VSCs. Fig. 6 shows that individual decentralized controllers underestimate the disturbance due to the large electrical distance from the fault location, with VSC at bus 1 being the only one to react, however, insufficiently to compensate the disturbance and prevent load-shedding. The enhanced controller on the other hand correctly estimates the disturbance and reacts appropriately with all available units.

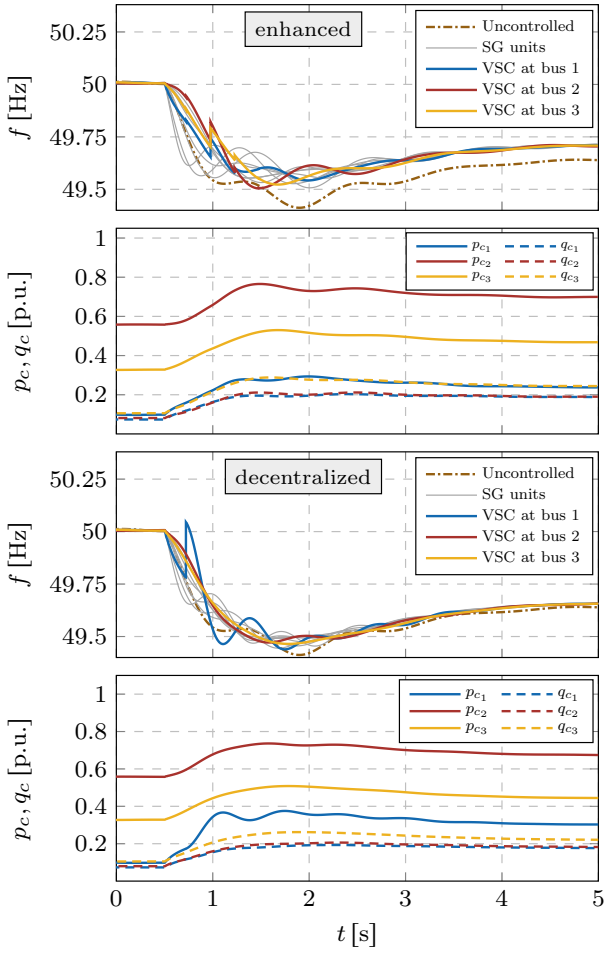

Fig. 6. Individual unit frequency responses for the enhanced (top) and decentralized (bottom) FFC shemes following a disturbance at bus 38.

V. CONCLUSION

The paper introduces a novel FFC scheme for frequency containment in low-inertia systems using *grid-forming* VSCs with controllable DC-side storage. A supervisory control layer consisting of an MPC-based controller and a data-driven observer manipulates the active power setpoints in response to a disturbance. A frequency prediction model with SVM regression disturbance estimator is employed to accurately predict the system frequency evolution. The performance of the controller was compared to a recently developed decentralized FFC scheme. Unlike the decentralized approach, the enhanced controller obtains an accurate disturbance estimate independent of the disturbance location and hence, operates with low error margins. However, with cost of the additional communication effort. Future work will focus on the optimal placement and sizing of inverter units with battery storage in order to minimize the investment costs for provision of FFC while ensuring frequency containment in large number of disturbance scenarios.

REFERENCES

[1] F. Milano, F. Dörfler, G. Hug, D. J. Hill, and G. Verbič, "Foundations and challenges of low-inertia systems," in *Power Systems Computation Conference (PSCC)*, Jun 2018, pp. 1–25.

[2] Q. Hong *et al.*, "Fast frequency response for effective frequency control in power systems with low inertia," *The Journal of Engineering*, vol. 2019, no. 16, pp. 1696–1702, 2019.

[3] Q. C. Zhong and G. Weiss, "Synchronverters: Inverters that mimic synchronous generators," *IEEE Transactions on Industrial Electronics*, vol. 58, no. 4, pp. 1259–1267, April 2011.

[4] U. Markovic, O. Stanojev, P. Aristidou, and G. Hug, "Partial grid forming concept for 100% inverter-based transmission systems," in *IEEE PES General Meeting*, Aug 2018, pp. 1–5.

[5] M. A. Torres, L. A. C. Lopes, L. A. Moran, and J. R. Espinoza, "Self-tuning virtual synchronous machine: A control strategy for energy storage systems to support dynamic frequency control," *IEEE Transactions on Energy Conversion*, vol. 29, no. 4, pp. 833–840, Dec 2014.

[6] U. Markovic, N. Früh, P. Aristidou, and G. Hug, "Interval-Based Adaptive Inertia and Damping Control of a Virtual Synchronous Machine," in *2019 PowerTech*, Jun 2019, pp. 1–6.

[7] U. Markovic, Z. Chu, P. Aristidou, and G. Hug, "LQR-based adaptive virtual synchronous machine for power systems with high inverter penetration," *IEEE Transactions on Sustainable Energy*, vol. 10, no. 3, pp. 1501–1512, 2019.

[8] M. Ashabani and Y. A. R. I. Mohamed, "Novel comprehensive control framework for incorporating VSCs to smart power grids using bidirectional synchronous-VSC," *IEEE Transactions on Power Systems*, vol. 29, no. 2, pp. 943–957, March 2014.

[9] J. Rawlings, D. Mayne, and M. Diehl, *Model Predictive Control: Theory, Computation, and Design*. Nob Hill, 2017.

[10] L. Papangelis, M.-S. Debry, T. Prevost, P. Panciatici, and T. V. Cutsem, "Decentralized model predictive control of voltage source converters for ac frequency containment," *International Journal of Electrical Power & Energy Systems*, vol. 98, pp. 342 – 349, 2018.

[11] O. Stanojev, U. Markovic, P. Aristidou, G. Hug, D. S. Callaway, and E. Vrettos, "MPC-Based Fast Frequency Control of Voltage Source Converters in Low-Inertia Power Systems," *IEEE Transactions on Power Systems*, pp. 1–1, 2020.

[12] U. Tamrakar, T. M. Hansen, R. Tonkoski, and D. A. Copp, "Model predictive frequency control of low inertia microgrids," in *2019 IEEE 28th International Symposium on Industrial Electronics (ISIE)*, June 2019, pp. 2111–2116.

[13] A. Ulbig, T. Rinke, S. Chatzivasileiadis, and G. Andersson, "Predictive control for real-time frequency regulation and rotational inertia provision in power systems," in *52nd IEEE Conference on Decision and Control*, 2013, pp. 2946–2953.

[14] U. Markovic, O. Stanojev, E. Vrettos, P. Aristidou, D. Callaway, and G. Hug, "Understanding Stability of Low-Inertia Systems," *engrXiv*, 2019. [Online]. Available: engrxiv.org/jwzrq

[15] E. Ekomwenrenren, H. Alharbi, T. Elgorashi, J. Elmirghani, and P. Aristidou, "Stabilising control strategy for cyber-physical power systems," *IET Cyber-Physical Systems: Theory Applications*, vol. 4, no. 3, pp. 265–275, 2019.

[16] A. J. Smola and B. Schölkopf, "A tutorial on support vector regression," *Statistics and Computing*, vol. 14, no. 3, p. 199–222, Aug. 2004.

[17] T. Athay, R. Podmore, and S. Virmani, "A practical method for the direct analysis of transient stability," *IEEE Transactions on Power Apparatus and Systems*, vol. PAS-98, no. 2, pp. 573–584, March 1979.